Electron-impact ionization of hydrogenlike ions in QED theory

Hsiao-Ling Sun,[1] Jyh-Ching Chang,[2] Ju-Tang Hsiao,[3] Sheng-Fang Lin,[4] and Keh-Ning Huang[1,4]

[1]*Institute of Atomic and Molecular Sciences, Academia Sinica, Post Office Box 23-166, Taipei, Taiwan 106, Republic of China*

[2]*Department of Science Education, National Hsinchu Teachers College, Hsinchu, Taiwan 300, Republic of China*

[3]*Department of Natural Sciences, National Institute for Compilation and Translation, Taipei, Taiwan 106, Republic of China*

[4]*Department of Physics, National Taiwan University, Taipei, Taiwan 106, Republic of China*

(Received 21 January 2010; published 27 April 2010; publisher error corrected 4 May 2010)

Relativistic cross sections for electron-impact ionization including quantum electrodynamic effects are studied for hydrogenlike ions in the two-potential formalism. Results are compared with other theoretical calculations and experimental data. Effects of the transverse-photon interaction as well as vacuum polarization potential between charges are analyzed. Systematic behaviors along the H-isoelectronic sequence are summarized.

DOI: 10.1103/PhysRevA.81.042711 PACS number(s): 34.80.Dp

I. INTRODUCTION

Electron-impact ionization is one of the major fundamental processes for understanding the atomic structure and collision mechanisms. Knowledge of ionization cross sections has applications in astrophysics, plasma physics, and radiation physics. In particular, the electron-impact ionization cross sections for highly charged ions are important in the study of high-temperature plasmas. However, obtaining extensive data on ionization cross sections of highly charged ions is difficult in both theory and experiment.

The cross sections of electron-impact ionization for U^{91+}-U^{90+} were first measured by Claytor *et al.* [1] at 222 keV electron energy in the heavy-ion channeling experiment. Marrs *et al.* [2,3], O'Rourke *et al.* [4], and Watanabe *et al.* [5] obtained the electron-impact ionization cross sections for some intermediate- and high-Z hydrogenlike ions in electron-beam ion trap experiments. Donets and Ovsyannikov [6] measured the ionization cross sections for Ne^{9+} and Ar^{17+}. Among theoretical calculations, the direct electron-impact-ionization cross sections for U^{91+} and U^{90+} were evaluated in the lowest-order quantum electrodynamics (QED) by Pindzola *et al.* [7] and for hydrogenic ions with nuclear charge Z between 26 and 92 by Moores and Pindzola [8] using a relativistic distorted-wave method. Electron-impact ionization for U^{91+} including exchange effects are later calculated by Pindzola *et al.* [9]. Moores and Reed [10] investigated the effects of the transverse-photon interaction in the relativistic distorted-wave calculations for high-Z hydrogenlike ions. Ionization cross sections for a variety of ions with one to four bound electrons and nuclear charge Z from 10 to 92 has been studied by Fontes *et al.* [11] in the relativistic distorted-wave approximation including the transverse-photon interaction for incident electron energies up to about 6 units of ionization energy.

A complete kinematic analysis of impact-ionization processes has been presented by Huang [12], in which all dynamical parameters are given in terms of reduced matrix elements. By the two-potential formalism, relativistic cross sections of electron- and positron-impact ionizations of hydrogen-, helium-, lithium-, and berylliumlike ions have been reported by Kao *et al.* [13], Hsu *et al.* [14], Kuo *et al.* [15],Chang *et al.* [16], Szuma [17], Huang *et al.* [18],Sun [19], Kuo and Huang [20,21], and Chang *et al.* [22].

In this work, we apply the two-potential formalism to calculate electron-impact ionization cross sections of hydrogenlike ions with QED effects. In Sec. II we present the general theory of electron-impact ionization in the two-potential formalism. The interaction Hamiltonians for the ionization processes and the transition matrix elements in terms of radial integrals for hydrogenlike targets are given in Sec. II. Numerical results and discussions are provided in Sec. III, and the conclusion is made in Sec. IV.

II. THEORY

A. Kinematic analysis

In electron-impact ionization processes, the target ion is ionized by an incident electron of linear momentum $\mathbf{k}_i$ and energy E_i, and the two emerging electrons are described by $(\mathbf{k}_p, E_p)$ and $(\mathbf{k}_s, E_s)$, where the primary (faster) electron is specified by subscript p and the secondary (slower) electron by subscript s. By energy conservation, we have

$$E_i + E_b = E_p + E_s, \tag{1}$$

where E_b is the energy of the bound electron.

If both the incident electron and the target ion are unpolarized, the triple-differential cross section in a relativistic formulation have been given by Huang [12] in atomic units as

$$\frac{d^3\sigma}{dE_s d\Omega_p d\Omega_s} = \frac{(2\pi)^4}{c^6}\left[\frac{k_p E_p k_s E_s E_i}{k_i}\right]\sum_{(fi)}|T_{fi}|^2, \tag{2}$$

where c is the speed of light, T_{fi} is the appropriate transition amplitude, and the summation over (fi) denotes symbolically averaging over the initial and summing over the final polarizations. The single differential cross section is obtained by integrating over Ω_p and Ω_s as

$$\frac{d\sigma}{dE_s} = \frac{(2\pi)^4}{c^6}\left[\frac{k_p E_p k_s E_s E_i}{k_i}\right]\int d\Omega_p \int d\Omega_s \sum_{(fi)}|T_{fi}|^2$$

$$= \frac{2\pi^3}{k_i^2(2J_b+1)}\sum_{\alpha} d_\alpha^2, \tag{3}$$

where J_b is the total angular momentum of the target, and the summation is over all possible channels denoted by the index

$\alpha \equiv (\kappa_i,\kappa_p,\kappa_s,j,J)$. Here the real amplitude d_α is defined by the reduced matrix element of the partial wave amplitude in channel α,

$$d_\alpha \exp(i\delta_\alpha) = i^{l_i-(l_p+l_s)} \exp[i(\sigma_{\kappa_p}+\sigma_{\kappa_s})] \times \langle \alpha^-[J_\alpha(j_p j_s)j]J \| H_I \| (j_b j_i)J\rangle, \quad (4)$$

where σ_{κ_p} and σ_{κ_s} denote the Coulomb phase shifts of the two outgoing electrons, J_α and J the total angular momentum of the residual ion and of the entire collision complex, respectively, and H_I the appropriate interaction Hamiltonian.

The total cross section is obtained by integrating over E_s as

$$\sigma = \int_{c^2}^{(E_i+E_b)/2} \frac{d\sigma}{dE_s} dE_s, \quad (5)$$

where c^2 represents the rest energy of the electron.

B. Two-potential formulation

The total Hamiltonian H of the projectile-target system can be separated into two parts:

$$H = H_i + V_i, \quad (6)$$

where H_i is the unpertubered Hamiltonian before the collision and V_i is the interaction potential between the projectile and the target during the collision.

In collision theory, the transition matrix element T_{fi} of electron-impact ionization is given in the prior form by

$$T_{fi} = \langle \Psi_f^{(-)}|V_i|\Phi_i\rangle - \langle P\Psi_f^{(-)}|V_i|\Phi_i\rangle, \quad (7)$$

where the first and second terms are the direct and exchange terms, respectively, and Φ_i is the eigenstate of H_i and $\Psi_f^{(-)}$ is the eigenstate of H with the incoming-wave boundary condition. Here the symbol P denotes the permutation between electrons.

In the two-potential formulation, we separate the inetraction potential V_i into the distorting potential U_i and the residual potential W_i as

$$V_i = U_i + W_i. \quad (8)$$

We can therefore reduce the transition matrix elements (8) into the two-potential form as

$$T_{fi} = \langle \Psi_f^{(-)}|W_i|\psi_i^{(+)}\rangle - \langle P\Psi_f^{(-)}|W_i|\psi_i^{(+)}\rangle, \quad (9)$$

where $\psi_i^{(+)}$ denotes the wave function in the distorting potential U_i.

C. Interaction Hamiltonians

In the relativistic theory, the unperturbed Hamiltonian H_i and the interaction potential V_i are written as

$$H_i = (c\boldsymbol{\alpha}_1\cdot\mathbf{p}_1 + c^2\beta_1) + (c\boldsymbol{\alpha}_2\cdot\mathbf{p}_2 + c^2\beta_2) + V_n(r_2), \quad (10)$$

$$V_i = V_n(r_1) + V(r_{12}), \quad (11)$$

where $\boldsymbol{\alpha}_i$ and β_i are Dirac matrices and the indices 1 and 2 refer, respectively, to the incident and bound electrons before the collision as well as the scattered and ejected electrons after the collision. Here $V_n(r_i)$ is the nuclear potential of the form

$$V_n(r) = \begin{cases} -\dfrac{Z}{2R}\left(3-\dfrac{r^2}{R^2}\right), & r \leqslant R, \\ -\dfrac{Z}{r}, & r > R, \end{cases} \quad (12)$$

where R is the radius of a uniformly charged nucleus.

The potential $V(r_{12})$ in (11) stands for the electron-electron potential in the QED theory in various levels of approximation, for example, the Coulomb interaction or the Coulomb interaction plus the transverse-photon interaction. These interactions between charges are due to the exchange of four types of photons, namely, one timelike photon, one longitudinal photon, and two transverse photons, which are referred to as the covariant-photon interaction in totality. The exchange of the timelike and longitudinal photons together leads to the instantaneous Coulomb interaction. The transverse-photon interaction [23,24] refers to the exchange of two types of transverse photons.

In addition, processes involving the creation of virtual electron-positron pairs by the photon field produce the vacuum-polarization potential between charges. The lowest-order vacuum-polarization potential, known as the Uehling potential, may be expanded for a spherical charge distribution in a convergent form valid for all distances [25]. The ratios of vacuum-polarization potentials of various orders to the Coulomb potential for a point nucleus have been evaluated by Huang [25] for $r \leqslant 1351.6$ fm, where the Uehling potential falls to less than 0.1 ppm of the Coulomb potential.

Because in the initial state the incident electron is generally screened by the bound electron, we may choose U_i and W_i in (8) as

$$U_i = V_n(r_1) + v_i(r_1), \quad (13)$$

$$W_i = V(r_{12}) - v_i(r_1). \quad (14)$$

Here the average potential $v_i(r_1)$ is due to the wave function $\Phi_0(\mathbf{r}_2)$ of the bound electron of the hydrogenlike target,

$$v_i(r_1) = \langle \Phi_0(\mathbf{r}_2)|\frac{1}{r_{12}}|\Phi_0(\mathbf{r}_2)\rangle. \quad (15)$$

D. Transition matrix elements

The wave function $\psi_i^{(+)}$ in (9) can be expressed as

$$\psi_i^{(+)} = \chi_i^{(+)}(\mathbf{r}_1)\Phi_0(\mathbf{r}_2). \quad (16)$$

Here the distorted wave function $\chi_i^{(+)}$ for the incident electron with the outgoing-wave boundary condition satisfies the equation

$$(c\boldsymbol{\alpha}_1\cdot\mathbf{p}_1 + c^2\beta_1 + U_i - E_i)\chi_i^{(+)}(\mathbf{r}_1) = 0. \quad (17)$$

As an approximation to the final-state wave function $\Psi_f^{(-)}$, we choose the distorted final-state wave function of product form as

$$\Phi_f^{(-)} \approx \chi_p^{(-)}(\mathbf{r}_1)\chi_s^{(-)}(\mathbf{r}_2), \quad (18)$$

where $\chi_p^{(-)}(\mathbf{r}_1)$ and $\chi_s^{(-)}(\mathbf{r}_2)$ satisfy the following equations:

$$(c\boldsymbol{\alpha}_1\cdot\mathbf{p}_1+c^2\beta_1+U_p-E_p)\chi_p^{(-)}(\mathbf{r}_1)=0, \tag{19}$$

$$(c\boldsymbol{\alpha}_2\cdot\mathbf{p}_2+c^2\beta_2+U_s-E_s)\chi_s^{(-)}(\mathbf{r}_2)=0. \tag{20}$$

Here the distorting potentials U_p and U_s are for the primary (faster) and secondary (slower) electrons, respectively. In the present calculation, we choose the model such that the primary electron is completely screened in the asymptotic region by the secondary electron, while the secondary electron is affected only by the Coulomb potential of the nucleus. This model works quite well away from the ionization threshold. Therefore, the distorting potentials U_p and U_s are given explicitly as

$$U_p(r_1)=V_n(r_1)+v_i(r_1), \tag{21}$$

$$U_s(r_2)=V_n(r_2). \tag{22}$$

By using a graphical method [26], we obtain an expression for the real transition matrix elements d_α of Eq. (4) in terms of $3n-j$ coefficients and radial integrals. The electron-electron interaction between two-particle configurations in the jm scheme has the general form [26]

$$\langle ab|V(r_{12})|cd\rangle = \int d^3r_1\int d^3r_2\, u_a^\dagger(1)\,u_b^\dagger(2)\,V(r_{12})\,u_c(1)\,u_d(2), \tag{23}$$

where a, b, c, and d indicate generally different Dirac orbitals with the form

$$u_{n\kappa m}(\mathbf{r})=\frac{1}{r}\begin{bmatrix} G_{n\kappa}(r)\Omega_{\kappa m}(\theta,\varphi)\\ i\,F_{n\kappa}(r)\Omega_{-\kappa m}(\theta,\varphi)\end{bmatrix}. \tag{24}$$

Here the radial functions $G_{n\kappa}$ and $F_{n\kappa}$ are the large and small components, respectively, and $\Omega_{\kappa m}(\theta,\varphi)$ are two-component normalized spherical spinors. The jm-scheme matrix element (23) may be reduced to a linear combination of radial integrals suitable for numerical computations [26]:

$$\langle ab|V(r_{12})|cd\rangle=\sum_j G_j(ab;cd)X_j(ab;cd). \tag{25}$$

Here the coefficient $G_j(ab;cd)$ relates to angular-momentum couplings of the interacting particles and is defined in terms of 3-jm symbols as

$$G_j(ab;cd)=\begin{pmatrix} j_a & j & m_c\\ m_a & m_c-m_a & j_c\end{pmatrix}\begin{pmatrix} j_b & m_d & m_c-m_a\\ m_b & j_d & j\end{pmatrix}. \tag{26}$$

The expression $X_j(ab;cd)$ is called the interaction strength with the general form

$$X_j(ab;cd)=C_j(ab;cd)I_j(ab;cd), \tag{27}$$

$$C_j(ab;cd)=(-)^{j_a+j_d}[(2j_a+1)(2j_b+1)(2j_c+1)(2j_d+1)]^{1/2}\times\begin{pmatrix} j_a & j & j_c\\ \frac{1}{2} & 0 & -\frac{1}{2}\end{pmatrix}\begin{pmatrix} j_b & j & j_d\\ \frac{1}{2} & 0 & -\frac{1}{2}\end{pmatrix}, \tag{28}$$

where $I_j(ab;cd)$ is defined in terms of radial integrals, depending on the specific form of $V(r_{12})$. In the following, we summarize the results for various interactions.

(i) Coulomb interaction, $1/r_{12}$:

$$I_j(ab;cd)=-\langle W_{ac}R_jW_{bd}\rangle^{\text{even}}, \tag{29}$$

which has the explicit form

$$\langle W_{ac}R_jW_{bd}\rangle^{\text{even}}=\int_0^\infty dr_1\int_0^\infty dr_2 W_{ac}(r_1)R_jW_{bd}(r_2), \tag{30}$$

with

$$W_{\alpha\beta}(r)=G_\alpha(r)G_\beta(r)+F_\alpha(r)F_\beta(r),$$
$$R_j=r_<^j/r_>^{j+1}.$$

Here the superscript in the notation $\langle\ \rangle^{\text{even(odd)}}$ denotes the selection rule that both (l_a+j+l_c) and (l_b+j+l_d) have to be even (odd).

(ii) Transverse-photon interaction, $-(\boldsymbol{\alpha}_1\cdot\boldsymbol{\alpha}_2)\frac{e^{i\omega r_{12}}}{r_{12}}+(\boldsymbol{\alpha}_1\cdot\boldsymbol{\nabla}_1)(\boldsymbol{\alpha}_2\cdot\boldsymbol{\nabla}_2)[\frac{e^{i\omega r_{12}}-1}{\omega^2 r_{12}}]$:

$$\begin{aligned} I_j(ab;cd)&=-(1-\delta_{j0})(\kappa_a+\kappa_c)(\kappa_b+\kappa_d)\frac{(2j+1)}{j(j+1)}\langle V_{ac}g_jV_{bd}\rangle^{\text{odd}}\\ &\quad+(\kappa_c-\kappa_a)[\langle V_{ac}g_{j-1}P_{bd}\rangle^{\text{even}}-\langle V_{ac}g_{j+1}P_{bd}\rangle^{\text{even}}]\\ &\quad+j(j+1)[\langle P_{ac}s_jQ_{bd}\rangle^{\text{even}}-\langle Q_{ac}t_jP_{bd}\rangle^{\text{even}}], \end{aligned} \tag{31}$$

where

$$s_j=\begin{cases} -\dfrac{i}{r_1}j_{j+1}(\omega r_2)h_j(\omega r_1), & r_1>r_2,\\ \dfrac{r_1^{j-1}}{\omega^2 r_2^{j+2}}-\dfrac{i}{r_1}j_j(\omega r_1)h_{j+1}(\omega r_2), & r_1<r_2,\end{cases} \tag{32}$$

$$t_j=\begin{cases} \dfrac{r_2^{j-1}}{\omega^2 r_1^{j+2}}-\dfrac{i}{r_1}j_{j-1}(\omega r_2)h_j(\omega r_1), & r_1>r_2,\\ -\dfrac{i}{r_1}j_j(\omega r_1)h_{j-1}(\omega r_2), & r_1<r_2,\end{cases} \tag{33}$$

with j_j and h_j being the spherical Bessel and Hankel functions, respectively. In (30) the different combinations of radial functions are defined as

$$\begin{aligned} V_{\alpha\beta}(r)&=G_\alpha(r)F_\beta(r)+F_\alpha(r)G_\beta(r),\\ P_{\alpha\beta}(r)&=G_\alpha(r)F_\beta(r)-F_\alpha(r)G_\beta(r)+V_{\alpha\beta}(r)(\kappa_\beta-\kappa_\alpha)/j,\\ Q_{\alpha\beta}(r)&=-G_\alpha(r)F_\beta(r)+F_\alpha(r)G_\beta(r)\\ &\quad+V_{\alpha\beta}(r)(\kappa_\beta-\kappa_\alpha)/(j+1). \end{aligned} \tag{34}$$

III. RESULTS AND DISCUSSION

A. Total and single-differential cross sections

For comparative studies of total and single-differential cross sections of ions, we use the reduced cross sections defined as

$$\sigma_R\equiv\left(\frac{I}{I_H}\right)^2\sigma,$$
$$\frac{d\sigma_R}{du_s}\equiv\frac{I^3}{I_H^2}\frac{d\sigma}{dE_s}, \tag{35}$$

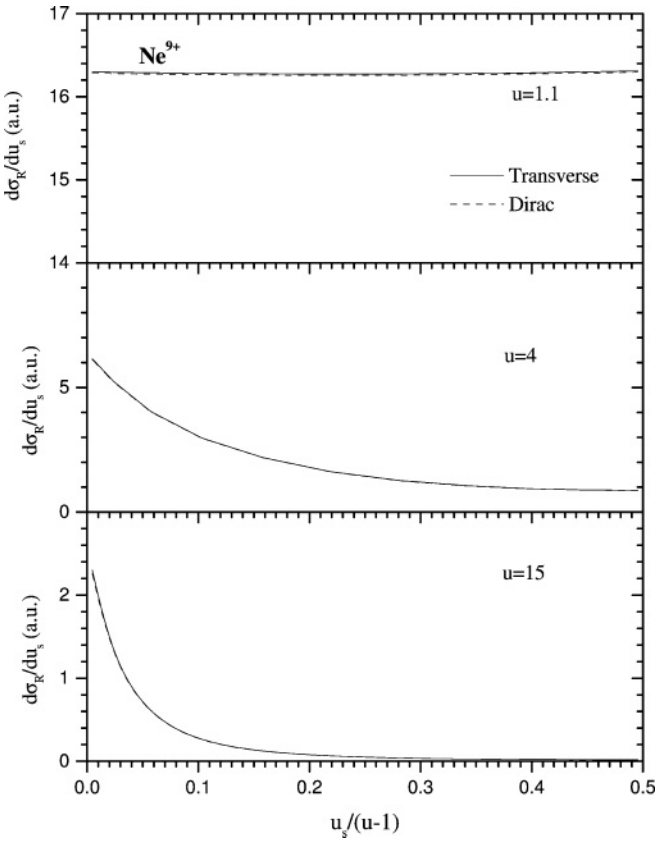

FIG. 1. Reduced single-differential cross sections in a.u. (a_0^2) for Ne^{9+} at incident energies $u = 1.1, 4$, and 15 in threshold energy units.

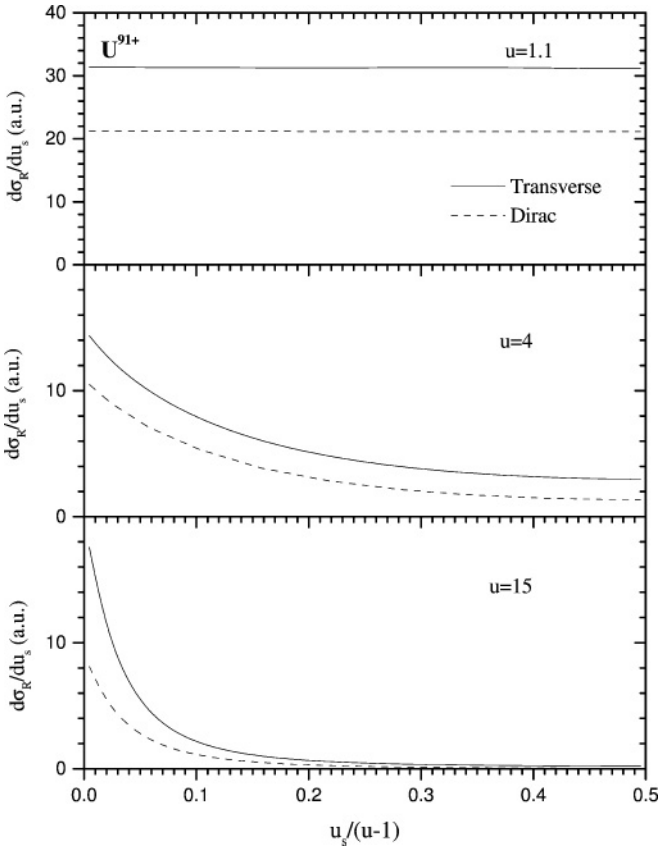

FIG. 2. Reduced single-differential cross sections in a.u. (a_0^2) for U^{91+} at incident energies $u = 1.1, 4$, and 15 in threshold energy units.

where $I = c^2[\sqrt{1-(Z\alpha)^2} - 1]$ denotes the ionization potential of the particular ion in consideration and I_H denotes that of the hydrogen atom. We shall also adopt the threshold-energy units $u = (E_i - c^2)/I$, $u_p = (E_p - c^2)/I$, and $u_s = (E_s - c^2)/I$ measured with respect to the rest energy of the electron. We have calculated cross sections for hydrogenlike ions with u ranging from 1.05 to 15. Results for selected ions Ne^{9+}, Ar^{17+}, Fe^{25+}, Mo^{41+}, Dy^{65+}, Au^{78+}, Bi^{82+}, and U^{91+} are plotted in Figs. 1–10 along with available experimental and theoretical data for comparison. In these figures, "Dirac" indicates cross sections with only Coulomb interaction between electrons and "Transverse" indicates cross sections with Coulomb plus transverse-photon interaction. The reduced cross sections (35) are given in atomic units throughout, that is, in units of a_0^2, where a_0 is the Bohr radius.

The single-differential cross sections for Ne^{9+} at $u = 1.1$, 4, and 15 are presented in Fig. 1, and those for U^{91+} in Fig. 2. Cross sections are almost constant at low incident energies for all ions, as exemplified in the case of $u = 1.1$ for Ne^{9+} and U^{91+}. These flat single-differential cross sections are due to the fact that Coulomb wave functions of the two outgoing electrons are insensitive to small variations in the momenta k_p and k_s near the ionization threshold. Therefore, all possible sharings of the available kinetic energy between the two outgoing electrons are almost equally probable. In Figs. 1 and 2, all curves at $u = 4$ and 15 decrease monotonically with u_s. We note particularly that the total cross section comes mainly from the low-u_s region at high incident energies. This can be explained by the properties of the Coulomb wave function, which can be written as

$$\phi(Z,\boldsymbol{k},\boldsymbol{r}) = (2\pi)^{-3/2} e^{\pi\eta/2} |\Gamma(1-i\eta)| \times e^{ik\cdot r}\, {}_1F_1(i\eta;1;ikr - i\boldsymbol{k}\cdot\boldsymbol{r}), \quad (36)$$

where $\eta = Z/k$ and k and ${}_1F_1$ are the momentum in the Coulomb potential of charge Z and the confluent hypergeometric function, respectively. The amplitude of the Coulomb wave function mainly depends on the parameter Z/k; therefore, it is insensitive to small absolute changes in k when the momentum is high. At high incident energies, the momentum k_p of the primary electron is generally high while the amplitude of the secondary-electron wave function decreases as k_s increases. Namely, an uneven sharing of the available kinetic energy $(u-1)$ is more favorable at high incident energies.

In Fig. 3, we show our total cross sections for Ne^{9+} and compare them with the theoretical Dirac results of Fontes *et al.* [11] and with the experimental data of Donets and Ovsyannikov [6]. The difference between our transverse and Dirac cross sections is small. The experimental results seem too large. Our total cross sections of Ar^{17+} are presented in Fig. 4 and in general agree with the experimental data of Donets and Ovsyannikov [6] and the theoretical Dirac results of Shi *et al.* [27]. In Fig. 5, we display our total cross sections of Fe^{25+}, which are compared with the results from theoretical Dirac calculation of Shi *et al.* [27] and experimental measurements by O'Rourke *et al.* [4]. The theoretical results are in good agreement with each other, while the measurements

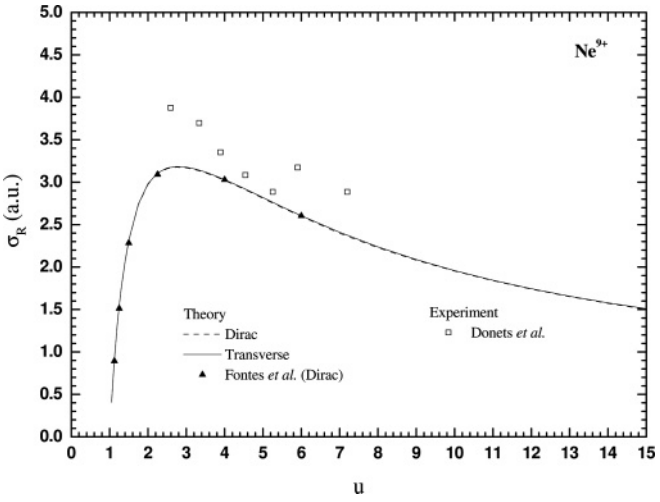

FIG. 3. Reduced total cross sections in a.u. (a_0^2) for Ne^{9+}.

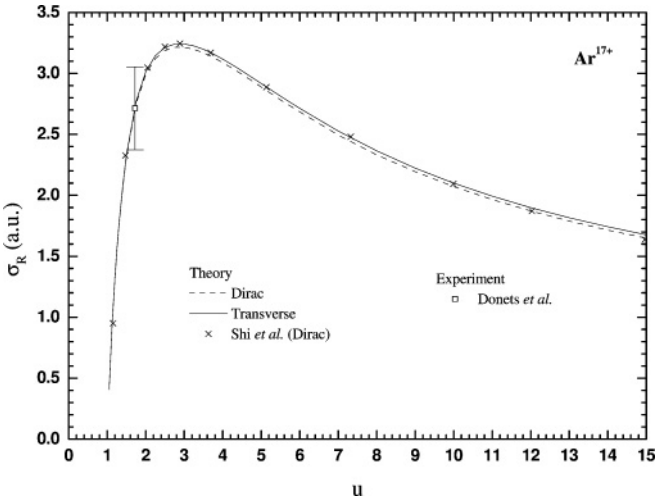

FIG. 4. Reduced total cross sections in a.u. (a_0^2) for Ar^{17+}.

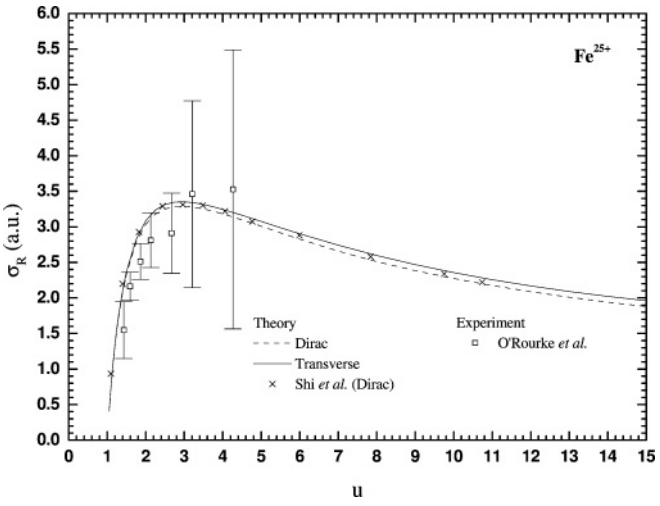

FIG. 5. Reduced total cross sections in a.u. (a_0^2) for Fe^{25+}.

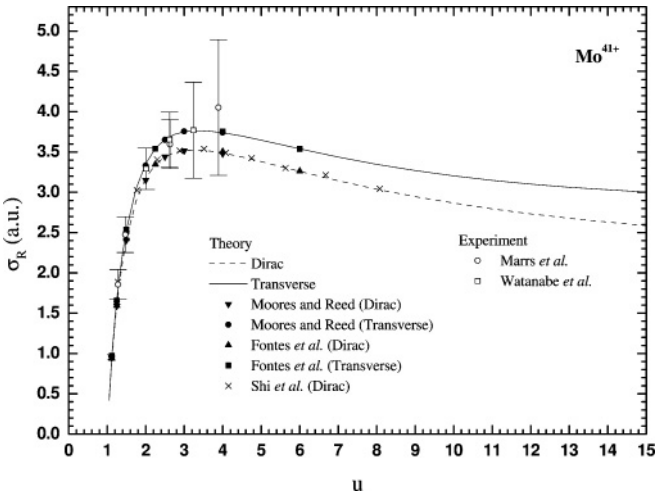

FIG. 6. Reduced total cross sections in a.u. (a_0^2) for Mo^{41+}.

of O'Rourke *et al.* are smaller than all theoretical calculations at low incident energies and approach our results at higher energies. Our calculation results of Mo^{41+} are presented in Fig. 6 and are compared with the theoretical Dirac and transverse results of Moores and Reed [10], Fontes *et al.* [11], and Shi *et al.* [27] and the experimental data by Marrs *et al.* [3] and Watanabe *et al.* [5]. It can be seen that our Dirac and transverse results in general agree well with other theoretical results and experimental data in all energy range.

In Figs. 7 and 8, we present our total cross sections of Dy^{65+} and Au^{78+}, and compare with the experimental data by Marrs *et al.* [3] and the theoretical data by Moores and Reed [10] and by Fontes *et al.* [11]. Our Dirac and transverse data are in fair agreement with the calculation of Moores and Reed, and Fontes *et al.* and Marrs' measurements coincide with our transverse data. Comparison for Bi^{82+} between our Dirac and transverse results, the theoretical calculations of Moores and Reed [10], and the experimantal data of Marrs *et al.* [3] are shown in Fig. 9. The transverse and Dirac cross sections of ours are in good agreement with Marrs' measurements and the Moores and Reed calculation. In Fig. 10, our total

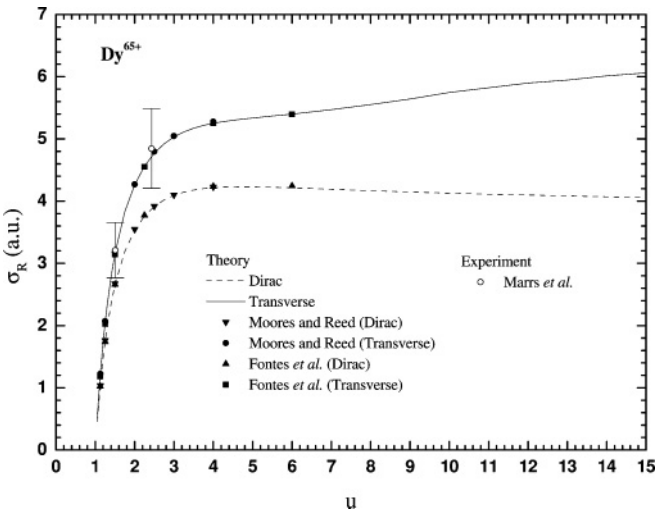

FIG. 7. Reduced total cross sections in a.u. (a_0^2) for Dy^{65+}.

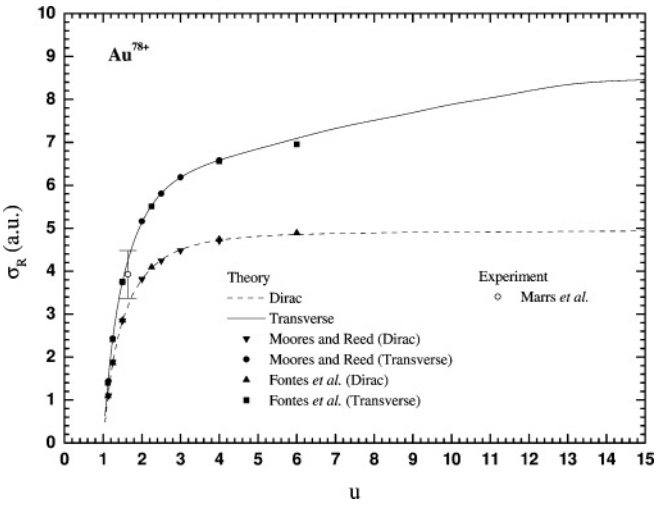

FIG. 8. Reduced total cross sections in a.u. (a_0^2) for Au^{78+}.

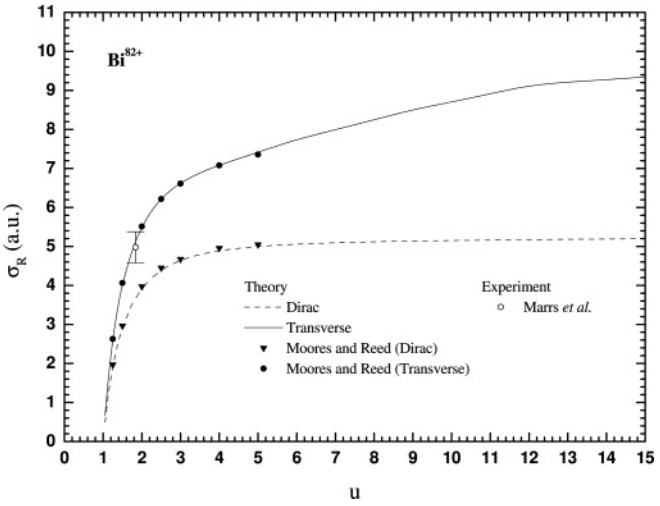

FIG. 9. Reduced total cross sections in a.u. (a_0^2) for Bi^{82+}.

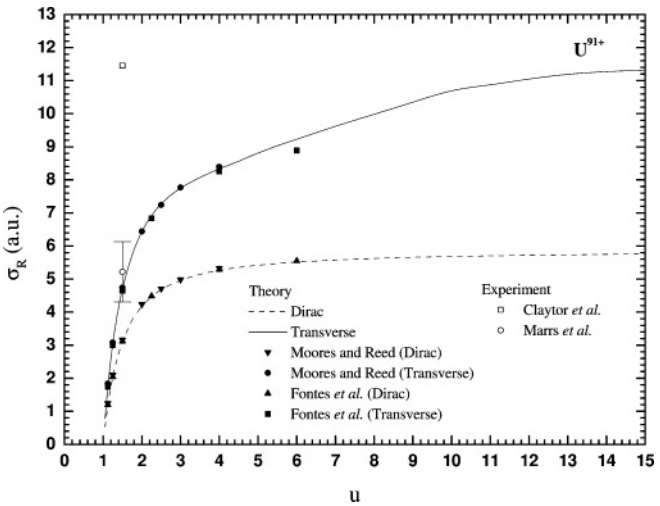

FIG. 10. Reduced total cross sections in a.u. (a_0^2) for U^{91+}.

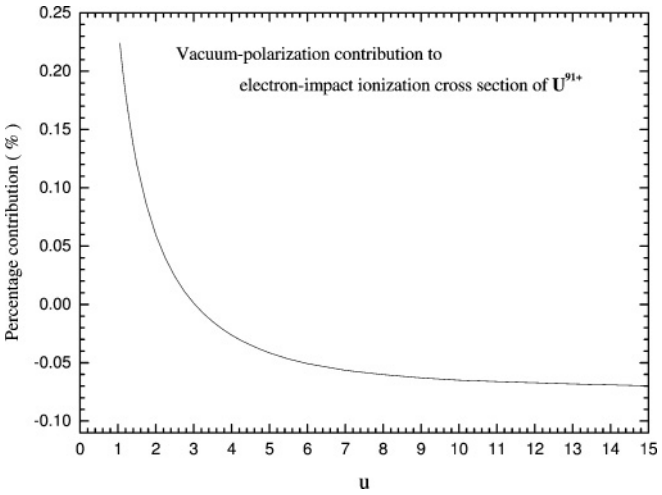

FIG. 11. The percentage contribution of the vacuum polarization to the total cross section for U^{91+} in electron-impact ionization.

cross sections of U^{91+} are compared with the experimental data of Claytor *et al.* [1] and Marrs *et al.* [2], as well as with the theoretical results of Moores and Reed [10] and Fontes *et al.* [11]. Our transverse data are within the error bars of the experimental value of Marrs *et al.* Our Dirac and transverse curves almost coincide with the data of Moores and Reed and Fontes *et al.*, except at higher incident energies where our transverse curve is slightly higher than other theoretical transverse data. Claytor's measurements at 222 keV remains a factor of two higher than all theoretical calculations.

According to our theoretical calculation, we found that the transverse-photon interaction increases ionization cross sections under 5% with $Z \leqslant 26$. The transverse cross sections are always larger than the Dirac calculation at all incident energies, even near threshold. The transverse-photon interaction increases ionization cross sections with increasing atomic number and with increasing incident energy.

The cross sections are also calculated for U^{91+} in Coulomb plus transverse-photon interaction with and without the vacuum-polarization potential between the electron and the nucleus. The percentage contribution of the vacuum-polarization potential to the cross section is plotted in Fig. 11. As expected, the vacuum-polarization effect contributes about one part per thousand to the ionization cross section [21].

B. Exchang effect

Exchange effects are quite substantial in electron-impact ionization of atoms and ions. The reduced transverse cross sections with and without exchange terms are compared for He^+, Ca^{19+}, Kr^{35+}, Xe^{53+}, Hf^{71+}, and U^{91+} in Fig. 12. We note that exchange effects raise the cross section near threshold and lower it as the excess energy increases for low- and intermidiate-Z ions, like He^+, Ca^{19+}, and Kr^{35+}. For highly charged ions, like Xe^{53+}, Hf^{71+}, and U^{91+}, exchange effects in general elevate the cross section at all incident energy regions.

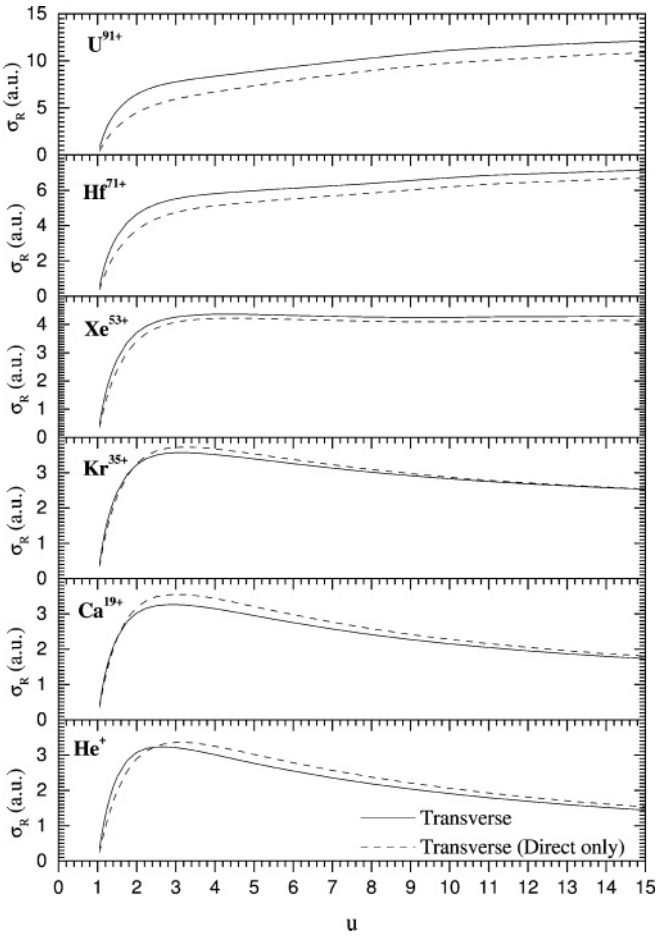

FIG. 12. Exchange effects in the reduced cross sections of He^{+}, Ca^{19+}, Kr^{35+}, Xe^{53+}, Hf^{71+}, and U^{91+}.

C. Scaling law and fit of ionization cross sections

In earlier studies of electron-impact ionization, Thomson's scaling law [28] by classical mechanics, $\sigma = 4(I_H/I)^2(1/u)(1-1/u)(\pi a_0^2)$, has provided a simple fitting formula to estimate ionization cross sections. An improved scaling law has been given as $\sigma = (1/u)(A\ln u + B)$ in the Bethe-Born theory, where A and B are constants. Moores and Nussbaumer [29] have attempted to include the relativistic effects by using the Mott-Massey formula,

$$\sigma = \frac{A}{u}\left\{\ln u + B - \ln\left(1-\frac{v^2}{c^2}\right) - \frac{v^2}{c^2}\right\}, \tag{37}$$

where v is the velocity of the incident electron. A relativistic form of the energies of incident electron is adopted in this formula. The parameter A may be determined from the photonionization cross section, and B by fitting to the Coulomb-Born results. Both A and B supposedly depend on the nuclear charge Z; however, they did not discuss the Z dependence of the parameters A and B along isoelectronic sequences. Recently, Fontes *et al.* [11] fitted their QED cross sections to a modified Mott-Massey formula,

$$\sigma = \frac{1}{u}\left\{A\ln u + D\left(1-\frac{1}{u}\right)^2 + Cu\left(1-\frac{1}{u}\right)^4 + \left[\frac{c}{u}+\frac{d}{u^2}\right] \times\left(1-\frac{1}{u}\right)\right\}\left(\frac{I_H}{I}\right)^2\frac{1}{141}\left[140+\left(\frac{Z}{20}\right)^{3.2}\right], \tag{38}$$

where coefficients A, D, c, and d are constants fitted by ion $Z = 20$, and parameter C is a function of Z.

In our previous work [13], nonrelativistic and relativistic cross sections with only Coulomb interaction have been studied along the H-isoelectronic sequence. Nonrelativistic cross-section curves approach a universal curve with increasing Z, while relativistic curves with QED effects have obvious deviations for high-Z ions from the universal curve.

In this work, we propose to fit the calculated reduced cross sections σ_R by a simple double series of $1/u$ and Z as

$$\sigma_R = \left(1-\frac{1}{u}\right)\sum_{m=0}^{4}\sum_{n=0}^{4} A_{mn}u^{-m}Z^n, \tag{39}$$

where A_{mn} can be represented by the 5×5 matrix $\mathbf{A}$, which is given as

$$\mathbf{A} = \begin{pmatrix} 2.313\,17(-1) & 7.290\,51(-3) & -6.348\,98(-5) & 3.459\,31(-5) & -1.842\,85(-7) \\ 2.175\,91(+1) & 5.272\,58(-3) & 3.646\,49(-3) & -3.026\,12(-4) & 2.067\,06(-6) \\ -3.609\,48(+1) & 1.052\,73(-2) & -2.074\,19(-2) & 1.196\,61(-3) & -8.330\,14(-6) \\ 4.299\,74(+1) & -6.684\,49(-1) & 5.897\,50(-2) & -2.194\,23(-3) & 1.499\,78(-5) \\ -2.127\,99(+1) & 7.459\,87(-1) & -4.615\,00(-2) & 1.357\,94(-3) & -9.024\,81(-6) \end{pmatrix}, \tag{40}$$

where the number n in the parenthesis (n) means the power of 10. The reduced cross sections σ_R of ions $2 \leqslant Z \leqslant 92$ are fitted for the incident-energy region $1.05 \leqslant u \leqslant 15$. The errors in the fitting are less than 1% in most cases and in general less than 2%. With the simple expansion matrix given in (40), we can predict rather accurately QED cross sections of hydrogenlike ions with $2 \leqslant Z \leqslant 92$ for a wide incident-energy range.

IV. CONCLUSION

A fully relativistic calculation of electron-impact ionization including Coulomb and transverse-photon interactions, as well as vacuum polarization potential for highly charged hydrogenlike ions, is performed. Exchange effects are included by antisymmetrizing the transition amplitude in the two-potential distorted-wave approximation. Contributions of

the vacuum-polarization potential are about at the one-part-per-thousand level in the Coulomb-plus-transverse-photon interaction. The total cross section is modified by exchange effects for all ions in wide energy region. The exchange terms increase the cross section in the transverse case at all incident energies for high-Z ions. QED effects are studied by comparison with the ionization cross section in only the Coulomb interaction and the Coulomb-plus-transverse-photon interaction. With increasing atomic number, QED effects become more and more important and enhance the single-differential and total cross sections even at lower incident energies. The QED reduced cross sections can be fitted by a simple double series expansion of $1/u$ and Z for a wide energy range. These fits are quite accurate within 1% in most cases by comparing with our calculations. Cross sections for ions with $2 \leqslant Z \leqslant 92$ along the H isoelectronic sequence can be derived easily and quickly by matrix in (40).

ACKNOWLEDGMENTS

This research work was supported in part by the National Science Council of the Republic of China under Grant No. NSC98-2112-M001-007.

[1] N. Claytor, B. Feinberg, H. Gould, C. E. Bemis Jr., J. Gomez del Campo, C. A. Ludemann, and C. R. Vane, Phys. Rev. Lett. **61**, 2081 (1988).
[2] R. E. Marrs, S. R. Elliott, and D. A. Knapp, Phys. Rev. Lett. **72**, 4082 (1994).
[3] R. E. Marrs, S. R. Elliott, and J. H. Scofield, Phys. Rev. A **56**, 1338 (1997).
[4] B. O'Rourke, F. J. Currell, H. Kuramoto, Y. M. Li, S. Ohtani, X. M. Tong, and H. Watanabe, J. Phys. B **34**, 4003 (2001).
[5] H. Watanabe, F. J. Currell, H. Kuramoto, S. Ohtani, B. E. O'Rourke, and X. M. Tong, J. Phys. B **35**, 5095 (2002).
[6] E. D. Donets and V. P. Ovsyannikov, Zh. Eksp. Teor. Fiz. **80**, 916 (1981).
[7] M. S. Pindzola, D. L. Moores, and D. C. Griffin, Phys. Rev. A **40**, 4941 (1989).
[8] D. L. Moores and M. S. Pindzola, Phys. Rev. A **41**, 3603 (1990).
[9] M. S. Pindzola, N. R. Badnell, D. L. Moores, and D. C. Griffin, Z. Phys. D **21**, S23 (1991).
[10] D. L. Moores and K. J. Reed, Phys. Rev. A **51**, R9 (1995).
[11] C. J. Fontes, D. H. Sampson, and H. L. Zhang, Phys. Rev. A **59**, 1329 (1999).
[12] K.-N. Huang, Phys. Rev. A **28**, 1869 (1983).
[13] H.-C. Kao, T.-Y. Kuo, H.-P. Yen, C.-M. Wei, and K.-N. Huang, Phys. Rev. A **45**, 4646 (1992).
[14] S.-W. Hsu, T.-Y. Kuo, C.-M. J Chen, and K.-N. Huang, Phys. Lett. A **167**, 277 (1992).
[15] T.-Y. Kuo, C.-M. J. Chen, S.-W. Hsu, and K.-N. Huang, Phys. Rev. A **48**, 357 (1993).
[16] J.-C. Chang, C.-M. Wei, T.-Y. Kuo, and K.-N. Huang, J. Phys. B **27**, 4715 (1994).
[17] L. Szuma, M.S. thesis, Department of Physics, National Taiwan University, 1994.
[18] K.-N. Huang, W.-Y. Cheng, and T.-Y. Kuo, J. Korean Phys. Soc. **32**, 232 (1998).
[19] H.-L. Sun, M.S. thesis, Department of Physics, National Taiwan University, 2001.
[20] T.-Y. Kuo and K.-N. Huang, Phys. Rev. A **64**, 032710 (2001).
[21] T.-Y. Kuo and K.-N. Huang, J. Phys. B **36**, 353 (2003).
[22] J.-C. Chang, H.-L. Sun, W.-Y. Cheng, and K.-N. Huang, Phys. Rev. A **69**, 052713 (2004).
[23] K.-N. Huang, Phys. Rev. A **18**, 1119 (1978).
[24] K.-N. Huang, J. Phys. B **11**, 787 (1978).
[25] K.-N. Huang, Phys. Rev. A **14**, 1311 (1976).
[26] K.-N. Huang, Rev. Mod. Phys. **51**, 215 (1979).
[27] X. H. Shi, C. Y. Chen, Y. Zhao, and Y. S. Wang, J. Quant. Spectrosc. Radiat. Transfer **91**, 161 (2005).
[28] M. R. H. Rudge, Rev. Mod. Phys. **40**, 564 (1968).
[29] D. L. Moores and H. Nussbaumer, J. Phys. B **3**, 161 (1970).